

# Preparation, characterization, and properties of graphene oxide/urushiol-formaldehyde polymer composite coating

Lei Zhang, Haitang Wu, Ming Wei, Zeyu Zheng, Dinh Duy Vu, Thi Tuyet Xuan Bui, Xiaohua Huang

© The Author(s) 2018

**Abstract** Graphene oxide (GO) was modified by 3-methacryloxypropyltrimethoxysilane (MPS) to obtain modified graphene oxide (MGO). MGO was dispersed in urushiol-formaldehyde polymer by mechanical mixing and ultrasonic dispersion, and MGO/urushiol-formaldehyde polymer (UFP) coatings with different MGO contents were fabricated. The microstructure, physico-mechanical properties, and electrochemical properties of the MGO/UFP composite coatings were investigated. The results indicated that the hardness, adhesion, and corrosion resistance of the MGO/UFP composite coatings were obviously enhanced compared with the pure UFP coatings. The hardness and the adhesion grade of the MGO/UFP composite coatings with 3.5 wt% MGO (GO, 1.5 wt%, and MPS, 2.0 wt%) reached 6H and 2, respectively. Additionally, GO connected with MPS by chemical bond and the well-dispersed MGO in UFP could significantly enhance the anticorrosion performance of the UFP coatings, which could result from bending the diffusion pathway of penetrant species in the UFP coating matrix.

**Keywords** Graphene oxide, Composite coating, Urushiol-formaldehyde polymer, Anticorrosion, Physico-mechanical properties

---

L. Zhang, H. Wu (✉), D. D. Vu,  
T. T. X. Bui, X. Huang (✉)  
College of Forestry, Northwest A&F University, 3 Taicheng  
Road, Yangling 712100, China  
e-mail: haitangwu@hotmail.com

X. Huang  
e-mail: 1067716566@qq.com

M. Wei, Z. Zheng  
Wuhan University of Technology, 122 Luo Shi Road,  
Wuhan 430070, China

## Introduction

Raw lacquer, a renewable raw resource derived from lacquer trees grown in the Asia region,<sup>1</sup> has been considered a promising natural coating material due to superior barrier properties against oxygen and water, good durability, chemical resistance, and mechanical properties. However, the shortcomings of slowly drying speed and poor workability of oriental lacquer form a major obstacle for its application. In view of this, it is necessary to modify raw lacquer or develop new lacquer-based materials. The urushiol-formaldehyde polymer (UFP) coating, a type of modified urushiol paint having excellent physical and chemical properties, was mainly developed for application in the coatings field with high properties, e.g., heavy anticorrosive properties.<sup>2–4</sup>

Nevertheless, the development of UFP suffers from several limitations due to the presence of low toughness and low alkaline resistance, which make it exhibit a poor membrane feature. In recent years, the superior properties of graphene oxide (GO) as a potential nanofiller for the polymer composite coating have attracted great attention by researchers in both academic and industrial fields. The astounding properties of GO for its application in the field of anticorrosion coating include remarkable liquid and gas barrier,<sup>5</sup> excellent chemical and thermal stability,<sup>6,7</sup> compelling mechanical stiffness and strength, and anticorrosion, antimicrobial, and antifouling features.<sup>8</sup> Therefore, GO has been successfully used as anticorrosive additives to improve the formulation of the polymer coatings and conventional organic coatings.<sup>9–11</sup> The development of GO-polymer-functionalized composite coatings is a potential method to effectively enhance anticorrosion properties and physico-mechanical properties of the coatings used for industrial equipment anticorrosion protection.<sup>12</sup> At present, the dispersibility of GO is a bottleneck for

the preparation of GO-polymer composite coatings, which strongly restricts its application in various fields. Physical dispersing methods such as ultrasonic dispersion can improve the dispersion of graphene in polymer to some extent.<sup>13</sup> Comparatively, chemical modification cannot only suppress the stacking and aggregation of GO, but also overcome the shortcoming of poor compatibility with polymers. To date, the modification of GO by grafting of chemical groups using silane such as vinyltris(2-methoxyethoxy)silane (TMEVS), 3-aminopropyltrimethoxysilane (APS), (3-aminopropyl)triethoxysilane (APTES),  $\gamma$ -(2,3-epoxypropoxy)propyltrimethoxysilane (GPTMS), and 3-methacryloxypropyltrimethoxysilane (MPS) has been applied in the preparation of nanocomposite.<sup>12,14–16</sup> The challenge is the option of the silane coupling agents to synthesize well-distributed silane-functionalized monolayer GO for the composite coatings.

In this work, modified graphene oxide/urushiol-formaldehyde polymer (MGO/UFP) coatings from raw lacquer were prepared in order to improve the physico-mechanical properties and enhance the corrosion resistance of the UFP coating. The effects of the type of silane coupling agents on the dispersion stability of graphene oxide in UFP were investigated. The effects of MGO content on the morphology, structural composition, and physico-mechanical properties of as-fabricated MGO/UFP composite coatings were discussed. Also, the corrosion resistance of the novel MGO/UFP composite coated onto tinplate was evaluated through electrochemical measurements and acid, alkali, and salt immersion tests. The potential application of the MGO/UFP composite coatings based on natural high polymer from raw lacquer was evaluated in the study.

## Materials and methods

### Materials

Raw lacquer sap was purchased from a local company located in AnKang, Shaanxi Province, China. The pure urushiol was obtained through xylene extraction, as described in the literature.<sup>17</sup> Potassium permanganate, sulfuric acid, hydrogen peroxide, hydrochloric acid, methanol, ethanol, acetone, xylene, aqueous ammonia solution, formaldehyde, vinyltris(2-methoxyethoxy)silane (TMEVS), (3-amino-propyl)-trimethoxysilane (APS), (3-aminopropyl)triethoxysilane (APTES), 3-methacryloxypropyltrimethoxysilane (MPS), and other chemical reagents were of analytical reagent grade. Graphite powder (particle size < 20  $\mu\text{m}$ ) was provided by Chinese Academy of Sciences Chengdu Organic Chemical Co., Ltd.

### Synthesis and dispersion stability of MGO suspension

Graphene oxide (GO) was synthesized according to modified Hummers method from natural graphite.<sup>18</sup> Four silane coupling agents (TMEVS, APS, APTES, and MPS) were used for the synthesis of MGO suspension. Typically, 0.05 g of the as-prepared GO was first dispersed in 5 mL of xylene as a solvent to form a suspension with concentration of 0.5 mg/mL by ultrasonication for 2 h. After that, MPS was added into the above as-obtained MGO suspension with xylene/MPS ratio of 50 and sonicated for 30 min. Then, the MGO suspension was prepared under vigorous stirring at room temperature for 30 min until a stable solution was achieved. Finally, the MGO suspension with the content of 1.0 wt% GO was typically prepared. The synthesis of MGO suspension using other silane coupling agents followed a similar procedure to the synthesis of MGO using MPS.

The effect of the type of silane coupling agents on the dispersion stability of the MGO suspension was investigated. The dispersion stability of the MGO suspension was determined using a WFZUV 2100 UV-Vis spectrophotometer (Formulation, France). The spectrophotometer detected the backscattering and transmission of monochromatic light ( $\lambda = 295 \text{ nm}$ ) through the samples. The experiment programs were as follows: GO/silane coupling agent suspension (20% w/w) was added into a centrifuge tube. Then, the GO/silane coupling agent suspension was conducted using 5415D centrifuge at 1000 rpm/min for 10 min. After that, the upper liquid of the GO/silane coupling agent suspension was diluted to 2000 times. The ratio of absorbance ( $R_{10}$ ) was calculated in accordance with the following equation<sup>19,20</sup>:

$$R_{10} = A_{10}/A_0 \times 100\%$$

in which  $R_{10}$  is the ratio of absorbance (%),  $A_0$  is the absorbance of the precentrifugal sample, and  $A_{10}$  is the absorbance after centrifugation 10 min. At the given equation, the higher the  $R_{10}$  value is, the better the stability.

### Synthesis of the GO/UFP and MGO/UFP composite coatings

GO/UFP and MGO/UFP composite coatings with different compositions were prepared by solution blending method (see Table 2). Urushiol-formaldehyde polymer (UFP) was synthesized according to described previously method.<sup>3</sup> In a typical procedure for the synthesis of MGO/UFP, 3.0 wt% of GO/MPS (1:2, w/w) was dispersed in 10 mL of xylene as a solvent through

ultrasonication for 120 min to achieve a uniform dispersion. Next, 10.0 g of UFP (UFP:MGO, 100:3) was added into the MGO suspension with xylene/MGO ratio of 100/3 (mL/w). Then, the solution was mixed at room temperature by a mechanical stirrer at 1000 rpm/min until getting a uniform dope solution. The synthesis of GO/UFP followed a similar procedure to that of MGO/UFP. The as-prepared GO/UFP and MGO/UFP samples were labeled as GU and MGU, respectively.

### *Preparation of the MGO/UFP composite films*

The liquid composite coatings were poured and painted on clean dried tinplate and glass sheets by roll coating method at ambient temperature, and the coated samples were kept at room temperature for 24 h before measurement. The films formed on tinplates with a size of 120 mm × 50 mm × 2 mm were used for mechanical tests including thickness, adhesion, and hardness. The films formed on tinplates with a size of 30 mm × 50 mm × 2 mm were used for the electrochemical impedance spectroscopy (EIS) test. Drying time and chemical corrosion-resistant properties of the samples were obtained using the glass sheets (60 mm × 20 mm × 2 mm). The films were peeled from the glass sheets (30 mm × 50 mm × 2 mm) by immersing into deionized water under 100°C for 5 min; then, the films were dried in a thermostatic drying oven at 120°C for 2.5 h to determine the cross-sectional and surface morphologies (SEM) and chemical state (XPS). In addition, the UFP film without GO and the GO/UFP film without silane coupling agent were also prepared on the tinplates and glass sheets as a reference sample.

### *Characterization of the MGO/UFP composite coatings*

The physico-mechanical property tests including thickness (coating thickness gauge), drying time (drying time tester), adhesion (QFD-type electric paint film adhesion tester), and hardness (QH-Q-type pencil hardness test apparatus) of the MGO/UFP composite coatings were performed.

The surface chemistry of the UFP, MGO/UFP, and GO/UFP coatings was analyzed by PerkinElmer FTIR spectroscopy and X-ray photoelectron spectroscopy (XPS). The FTIR test was carried out in the wavelength range of 400–4000  $\text{cm}^{-1}$ . The x-ray photoelectron spectroscopy (XPS) was obtained by a ThermoFisher Scientific ESCALAB K-Alpha spectrometer. The experiment program was as follows: Al Ka was used as the radiation source at a pressure of  $10^{-7}$  mbar under the voltage of 5 kV, and the shift of binding energies (BE) was calibrated with respect. The surface morphologies of the prepared coatings were examined by S-4800 field emission scanning electron microscopy (SEM, Hitachi Ltd., Japan) analysis. The phase crystallinity and composition of the prepared

coatings were measured by XRD (D8 Advance A25, Bruker). Cu Ka was used as the radiation source at the voltage of 40 kV and the emission current of 30 mA.

The thermostability of the prepared coatings was analyzed by a thermogravimetric analyzer (TGA/SDTA851<sup>o</sup>, Mettler-Toledo). In the TGA-DTG analysis, the temperature program was as follows: temperature region of 25–600°C, 10°C/min up to 600°C. Nitrogen was used as a carrier at a flow rate of 40 mL/min.

### *Chemical corrosion-resistant property*

In order to characterize the anticorrosive performance of the MGO/UFP composite coatings, the corrosive experiment in chemical solution was carried out. The coated glass plates as samples were immersed in 30%  $\text{H}_2\text{SO}_4$ , 10% NaOH, and 3% NaCl solution for 14 days at room temperature, and visual observations were carried out for the loss of light, color, or the formation of foam on the coatings surface. The samples were checked every 24 h, and images were recorded to validate the electrochemical impedance spectroscopy (EIS) results. The test was repeated twice as an electrochemical reference sample.

### *Electrochemical measurements*

Electrochemical impedance spectroscopy (EIS) and potentiodynamic polarization curve measurements were taken on a PGSTAT 30 electrochemical workstation using 3.5 wt% NaCl as the test solution and a three electrode as cell configuration for both Tafel plots and EIS tests: a platinum electrode as the counter electrode, a saturated calomel electrode (SCE) as the reference electrode, and the coated MGO/UFP tinplate sample as the working electrode with an exposed area of 1  $\text{cm}^2$ . The polarization curve tests were as follows: the applied potential between  $-0.25$  and  $+0.25$  V relative to open-circuit potential (OCP) at scan rate of 1 mV/s on 1  $\text{cm}^2$  anode. The EIS test was as follows: the frequency range of 0.01 Hz to 100 kHz using a sinusoidal voltage of 10 mV as the amplitude in order to minimize the external interference on the system.

## **Results and discussion**

### *The dispersion stability of the GO suspension*

The dispersion stability of the GO suspension by adding different silane coupling agents was investigated (Fig. 1). As can be seen from Fig. 1, the  $R_{10}$  values of all suspensions after 60-min ultrasonic-assisted treatment were ranked as follows: GO/TMEVS < GO/APTES < GO/APS < U < GO/MPS. Under the same GO content for all the samples, the greater the  $R_{10}$  value

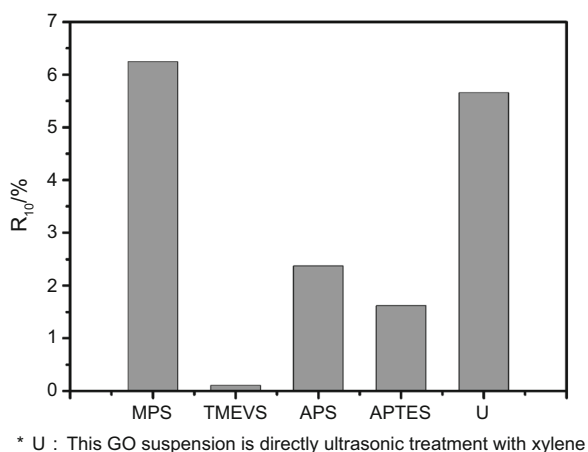


**Fig. 1: The absorbance ratios ( $R_{10}$ ) of  $A_{10}/A_0$  for the GO suspension using the UV/VIS spectrophotometer of different GO samples with different silane coupling agent. The  $A_{10}$  value corresponds to the centrifugal absorbance after 10 min related to GO suspension and  $A_0$  corresponds to the absorbance of the pre-centrifugal sample**

of GO/silane coupling agent suspension after ultrasonic treatment with xylene, the better the dispersion stability. The GO/MPS suspension with ultrasonic assistance showed the highest  $R_{10}$  value (6.25%) among the five GO suspensions. Meanwhile, the other  $R_{10}$  value of GO/TMEVS suspension with xylene was reduced to 0.11%, which corresponded to the lowest dispersion stability. It has been reported that silane coupling agent could be used for the functionalization of covalent bond of GO through the reaction between the hydroxyl group from the hydrolysis of siloxane and the hydroxyl group on the surface of GO, thus improving the stability of GO suspensions and the compatibility between GO and the organic polymer matrix.<sup>22</sup> GO/TMEVS exhibited the weakest dispersion stability, most likely due to its long carbon chain of silicon-alkoxy, leading to the slowest rate of hydrolysis reaction. The dispersion stability of GO/APTES was poorer than GO/APS and GO/MPS because the hydrolysis rate of ethoxy groups in APTES was slower than that of methoxy groups in APS and MPS.<sup>21</sup> Furthermore, it is noted that GO/APS showed poorer dispersion stability compared with GO/MPS. The possible reason was that the amino group in APS preferentially reacted with the carboxyl groups located on the edge of surface of GO, which inhibited the reaction between hydroxyl from the hydrolysis of APS and hydroxyl located on the surface of GO.<sup>22,23</sup> Further investigation would be needed to explore the mechanism in detail. In this work, comparing the results with other studies reported in the literature,<sup>13</sup> it was found that MPS grafting onto the GO surface was able to decrease the settling velocity of the GO suspension and GO spatial distributions might have a great significance for the suspension stability. As a result, MPS was chosen as a chemical modified additive since it played an

important role in subsequent interfacial interaction on the surface of UFP and graphene oxide.

### Characterization of the MGO/UFP composite coatings

#### FTIR analysis

As shown in Fig. 2a, after reacting with HCHO, several peaks intensity decreased in the spectrum of UFP compared with those of fresh urushiol. Peaks at 3500, 1180, and 1250  $\text{cm}^{-1}$  could be ascribed to the O–H stretching vibration and C–O and  $\beta_{\text{O–H}}$  stretching vibration, respectively, probably owing to the decrease in the number of the hydroxyl group on the phenyl ring and the formation of polymers corresponding to the hydroxyl group on the phenyl ring of urushiol.<sup>24</sup>

FTIR analysis was further carried out to verify the chemical grafting between GO and UFP. As shown in Fig. 2b, after chemical grafting of the GO with UFP, the intensities of the FTIR peaks of GO/UFP corresponding to the oxygen functionalities, such as the C=O stretching vibration peak at 1726  $\text{cm}^{-1}$ , the vibration and deformation peaks of O–H groups at 3395 and 1410  $\text{cm}^{-1}$ , respectively, the C–O (epoxy) stretching vibration peak at 1226  $\text{cm}^{-1}$ , and the C–O (alkoxy) stretching peak at 1052  $\text{cm}^{-1}$  decreased dramatically, and some of them disappeared entirely. The groups between most oxygen functionalities in the GO and hydroxy groups in UFP were removed, which confirmed that GO was successfully grafted onto the UFP polymer matrix through the chemical reaction.

Upon treatment with MPS, the C=O stretching vibration at 1733  $\text{cm}^{-1}$  in GO became obscured by the appearance of a stronger absorption at 1623  $\text{cm}^{-1}$  that could be attributed to C=O from MPS, as shown in Fig. 2b. The new bending and asymmetric vibrations at 1646, 958, and 571  $\text{cm}^{-1}$  could be assigned to Si–O–C, Si–OH, and Si–O–C bonds, respectively. The new band at 1096, 804, and 472  $\text{cm}^{-1}$  could originate from the silanes moieties tendency to self-reaction in the bulk of solution instead of GO surface and corresponded to the coupling of the Si–O–Si stretching vibration with the silanes deformation vibration (Fig. 2b), while those at 2800, 2770, and 2690  $\text{cm}^{-1}$  could be assigned to the stretching vibration of  $\text{CH}_2$ . Compared with typical  $\text{CH}_2$  bands (1350, 1465 and 2853, 2926  $\text{cm}^{-1}$ ), all the intensities of these bands were decreased, suggesting that it was characteristic of UFP with methylene groups. In addition, the characteristic peaks of UFP also appeared at 3370–3520  $\text{cm}^{-1}$  in the spectrum of MGO/UFP, all bands shifted to a low wave number and became broader, which demonstrated the successful crosslink between UFP and MGO for the formation of interpenetrating polymer networks at interfaces. Compared to the peaks of UFP, it was obvious from FTIR spectra that silane molecules bond grafted on GO surface through the chemical reaction

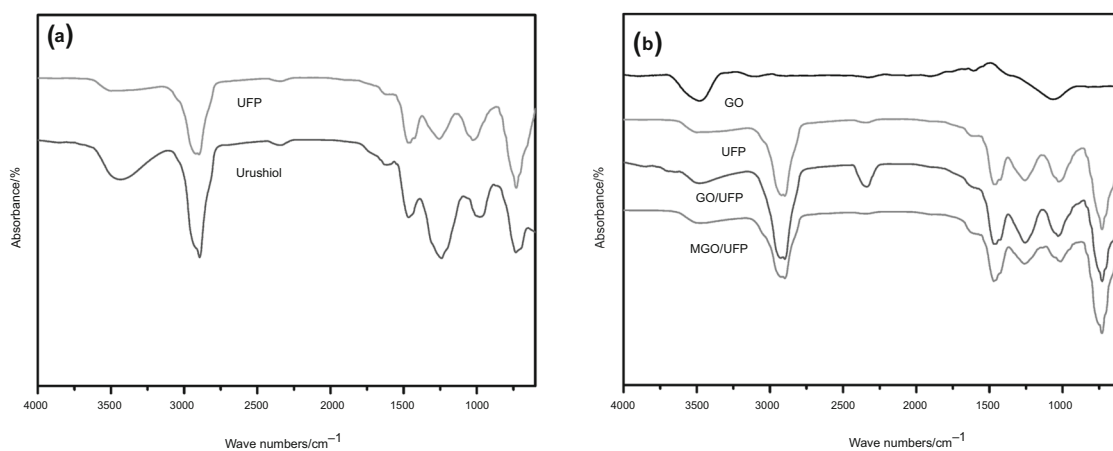


**Fig. 2:** FTIR spectra of neat UFP and urushiol (a), GO, UFP, GO/UFP and MGO/UFP (b) films

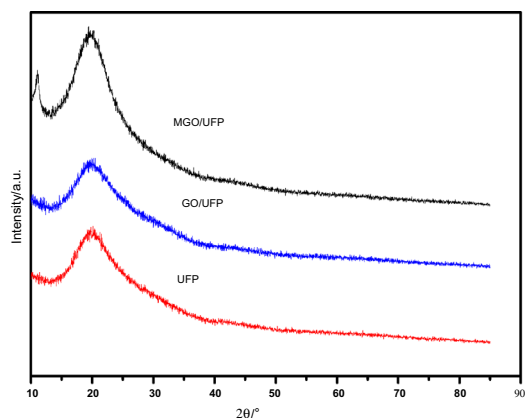


**Fig. 3:** XRD of the UFP, GO/UFP and MGO/UFP coating

with functional groups and higher amount of MGO crosslinked onto the UFP as polymer matrix.

#### *Phase composition of the MGO/UFP composite coatings*

XRD patterns of the UFP, GO/UFP, and MGO/UFP samples are given in Fig. 3. As can be seen, wide-angle X-ray diffraction showed a very broad peak at  $19.9^\circ$  owing to the presence of amorphous structure domains in the UFP films which was characteristic of UFP.<sup>25</sup> The XRD pattern of the GO/UFP sample was similar to that of the UFP, and no obvious characteristic diffraction peaks of GO were observed because of its low loading content and weak crystallization. Compared with the GO/UFP sample, the diffraction peaks at  $19.9^\circ$  of the MGO/UFP samples were sharp and intense, indicating their more highly crystalline nature than the GO/UFP sample.<sup>12</sup> This might be because graphene acting as nucleating agents promoted the heterogeneous nucleation of UFP polymer on the surface of MGO and further induced them to crystallize.

Similar findings have been reported in previous studies,<sup>26</sup> which showed that the addition of graphene nanosheets could efficiently accelerate the crystallization rate of polypropylene in graphene/polypropylene nanocomposites. Thus, incorporation of MGO into the UFP matrix tended to modify its crystallinity, which could eventually improve the tensile strength of the pure UFP films.<sup>27</sup>

Additionally, there were new decreased and diminished humps at  $2\theta = 10.9^\circ$ , indicating the presence of GO.<sup>12,28</sup> No impurity peaks were observed, confirming the high purity of the MGO/UFP films.

#### *Microstructure and chemical composition of the MGO/UFP composite coatings*

In this experiment, SEM micrographs in Fig. 4 show the bulk structural information on the MGO/UFP, GO/UFP, and pure UFP films. There was no visible agglomeration and protuberance or swelling behavior in the surface morphologies of the MGO/UFP (Fig. 4a) composite films by comparing with the GO/UFP composite films (Fig. 3c), indicating that the GO was well dispersed in the UFP since forming covalent bonding between MPS molecules and GO surface (hydroxyl on surface, carboxylic at edges and epoxide in the basal plane), which was similar to the one observed from the FTIR results.<sup>28</sup> After silane molecule-grafted reaction with graphene oxide, the images on some agglomerations in Fig. 4b of MGO/UFP composite samples were related to strong interfacial interaction of MGO with UFP polymer matrix and GO molecules were aggregated on UFP (Fig. 4c) compared to the smooth surface of the MGO/UFP composite film (Fig. 4a), which could demonstrate that the microstructure compactness of the MGO/UFP composite coatings can be improved to act as a barrier against corrosive agents and effectively protect base metal from corrosion.<sup>12,29,30</sup> Meanwhile, the incorpo-

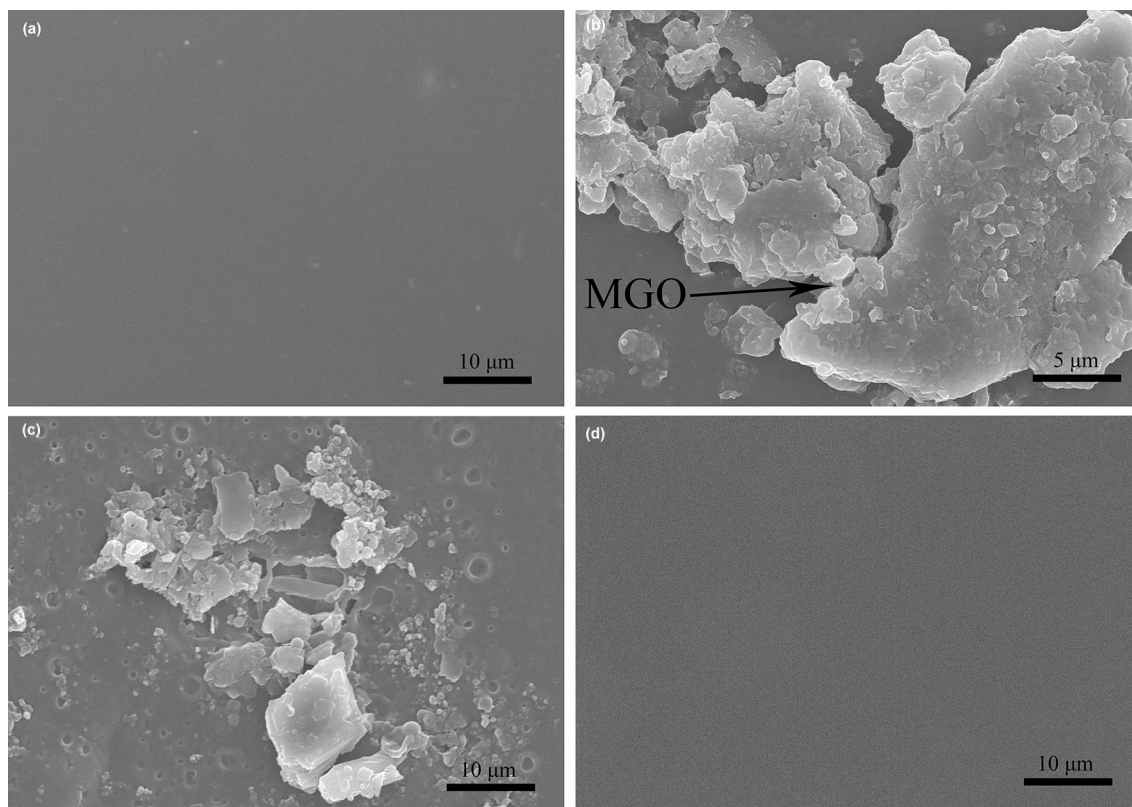


**Fig. 4:** SEM images from cross sections of (a) the MGO/UFP composite coatings on silicon chip substrate, (b) high magnification image of MGO/UFP coating, (c) the GO/UFP coating and (d) the pure UFP coating

ration of MGO suspension in the UFP was supposed to improve the surface adhesion of the UFP coatings by establishing a interfacial interaction between MGO and UFP.<sup>31</sup>

#### XPS analysis

The XPS analysis was carried out to determine the surface structure of the MGO/UFP composite coatings. The main structural information of the MGO/UFP composite films surface including O 1s, C 1s, and Si 2p are shown in XPS survey spectrum (Fig. 5a). The C 1s spectrum exhibited six contributions located at, respectively, 283.7, 284.8, 287.7, 285.6, 286.6, and 289 eV (Fig. 5b), which could be assigned to C–Si, C–C/C=C, C–O, C–O/C–O–Si, C–O–C, and O–C=O. The O 1s signals at, respectively, 530.2, 531.3, 532.2, 532.8, and 532.8 eV were related to five Gaussian–Lorentzian peaks including O–C=O, C=O, C–O/C–O–Si, Si–O–Si, and C–O–C/OH (Fig. 5c).<sup>5,9</sup> The Si 2p spectrum clearly evidenced the presence of two chemical environments for silicon atoms (Fig. 5d). The spectrum has been fitted by considering two resolved doublets (with a spin–orbit splitting between 2p<sub>3/2</sub> and 2p<sub>1/2</sub>). The first predominant doublet, present at 101.2 eV, is characteristic of Si–C. The second one, with a higher intensity, was located at higher binding energies,

102.3 eV, and corresponded with the FTIR results,<sup>32</sup> which confirmed that the MPS molecules were grafted on the GO surface in two forms of chemical bonding with hydroxyl and carboxylic functional groups. Meanwhile, it could be clearly found that these UFP polymer molecules completely crosslinked to MGO via interpenetrating polymer interface and forming a hydrogen bond. As can be seen from Table 1, the Si 2s signal, respectively, included 59.38% Si–O–Si and 40.62% Si–C peaks, which indicated that most of the silanes moieties successfully grafted onto the GO surface for the formation of the MGO/UFP composite coatings and these results were completely consistent with the FTIR analysis described above.<sup>28,33</sup>

#### Physico-mechanical properties of the MGO/UFP composite coatings

The study of the physico-mechanical properties involving thickness, drying time, adhesion, and hardness in the resulting composite coatings is essential for its application.<sup>2,34</sup> The physico-mechanical properties of the GO/UFP and MGO/UFP composite coatings with different GO content (GO, 0.5–2.0 wt%) were studied and are listed in Table 2. As can be seen, the addition of GO to the natural UFP significantly improved the adhesion and hardness at room temperature. The GO/

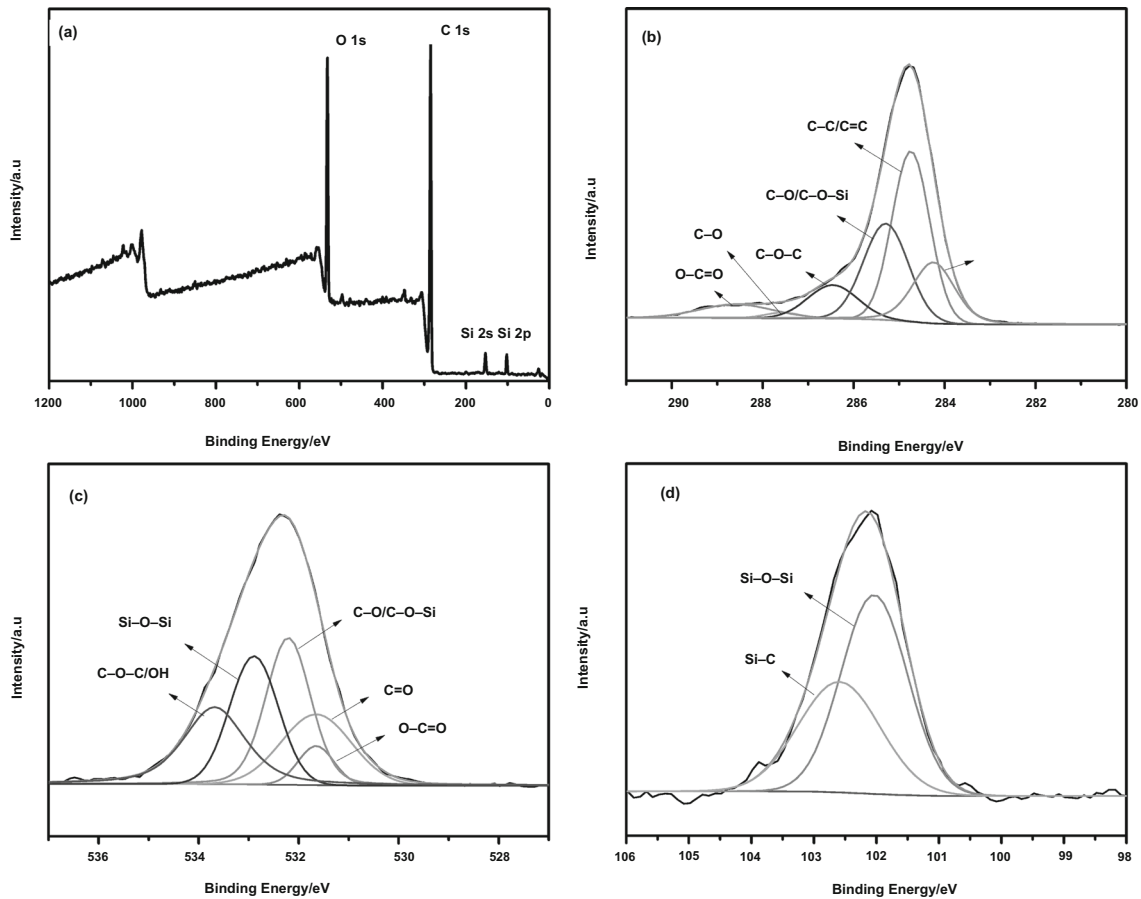


Fig. 5: (a) XPS survey spectrum and high resolution spectra of the MGO/UFP composite coatings (b) C 1s, (c) O 1s and (d) Si 2s

Table 1: The XPS results for the MGO/UFP composite sample

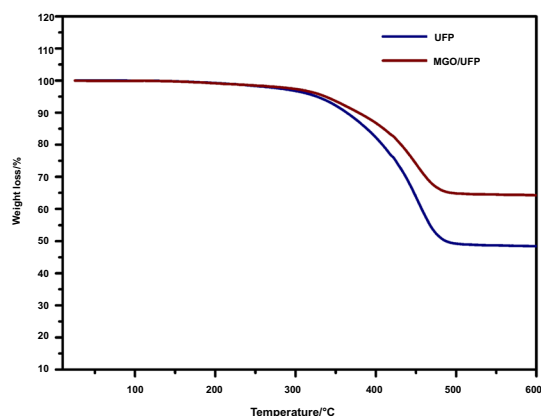
Signals	Bonds	Energy of bonds/eV	Components/%
C 1s	C-C/C=C	284.70	39.03
	C-O	287.60	1.20
	O-C=O	288.60	6.07
	C-O-C	286.50	10.18
	C-O/C-O-Si	285.30	26.22
	C-Si	284.20	17.31
	O 1s	O-C=O	531.65
O 1s	C=O	531.65	19.37
	C-O/C-O-Si	532.20	27.88
	Si-O-Si	532.90	24.43
	C-O-C/OH	533.70	22.83
Si 2s	Si-O-Si	102.00	59.38
	Si-C	102.60	40.62

UFP composite coatings consisting of 1.0 wt% GO could be more resistant to scratching up to grades of hardness and adhesion 5H and 1 than the neat UFP. On the basis of this finding, it could be concluded that

the incorporation of GO as reinforcement nanofillers had positively improved the hardness and adhesion.<sup>35</sup> The significant reinforcement was associated with interfacial interactions between the GO and UFP

**Table 2: Physico-mechanical properties of the GO/UFP and MGO/UFP composite coatings**

Sample	Composition			Hardness	Adhesion
	UFP	GO	MPS		
GU1	100	0.5	0	3H	3
GU2	100	1.0	0	5H	1
GU3	100	1.5	0	4H	1
GU4	100	2.0	0	4H	1
MGU1	100	0.5	2.0	4H	1
MGU2	100	1.0	2.0	5H	2
MGU3	100	1.5	2.0	5H	2
MGU4	100	2.0	2.0	6H	2
UFP	100	0.0	0.0	3H	3

**Fig. 6: TGA curves of the MGO/UFP composite films: UFP (GO, 0.0 wt.%) and MGO/UFP (GO, 1.0 wt.% and MPS, 2.0 wt.%)**

matrix, such as covalent bonds, van der Waals forces, and hydrogen bonding.<sup>2,36</sup> Nevertheless, the hardness of samples GU3 and GU4 was slightly reduced thereafter as the GO content further increased from 1.5 to 2.0 wt%. The decrease of physico-mechanical properties in GO/UFP should correspond to the nonuniform dispersion level (not optimal) and nanometer effect between GO and UFP matrix;<sup>37</sup> that is, a nonuniform distribution of GO particles will cause uneven stress in the composite films.<sup>2</sup> The MGO at higher concentration (GO, 2.0 wt%) slightly increased a grade of the hardness to 6H and slightly decreased a grade of the adhesion to 2 for sample MGU4, indicating that the large silane molecules MPS led to a better dispersion of GO in UFP for preventing the GO sheets from agglomeration. Moreover, the silane molecules reduced the hydrophilicity of the GO surface making it more compatible with the polymer matrix and the excess MGO could induce the interfacial interaction to form on the surface of the organic and the inorganic phases for UFP and GO.<sup>28,38</sup>

### Thermal properties of the MGO/UFP composite coating

Figure 6 shows the TGA curves of the UFP and MGO/UFP films. When the temperature was up to 600°C, the residual mass of UFP was only 45.66%. However, the residual mass of the MGO/UFP film was 64.53%, indicating the MGO/UFP coatings had superior thermal stability. It was also observed that the beginning thermal-decomposition temperature for the MGO/UFP composite coatings was slightly higher than the GO/UFP composite coatings due to the removal of oxygen functionalized groups from GO.<sup>33</sup> The main reason was the absence of oxygen functional groups after the GO modification process, which demonstrated that addition of MPS to the GO nanosheets could improve the thermal stability of the MGO/UFP composite coating during the whole decomposition process.

### Electrochemical measurements

#### Potentiodynamic Analysis

The effect of MGO content on the enhancement of the corrosion protection on metallic substrate coated with the pure UFP, GO/UFP, and MGO/UFP coatings was evaluated based on a corrosive medium (3.5 wt% NaCl aqueous solution) under potentiodynamic polarization conditions, as presented in Fig. 7, and the corresponding average values and the standard deviations of electrochemical parameters were extracted and are listed in Table 3. According to the results, when GO (1.0 wt%) was used as a chemically modified additive to UFP, the coated samples of GO/UFP displayed higher positive corrosion potentials ( $E_c$ , -460.51 mV) and lower corrosion current densities ( $i_c$ ,  $9.64 \times 10^{-9}$  A/cm<sup>2</sup>), indicating that the addition of GO significantly improved the anticorrosion resistance of the UFP coatings.<sup>39</sup> Moreover, the MGO/UFP (GO, 1.5 wt%) sample displayed the lowest  $i_c$  value ( $2.4 \times 10^{-9}$  A/cm<sup>2</sup>), suggesting that it could be provided with the highest corrosion resistance compared with other samples (GO content from 0.5 to 2.0 wt%). However, the corrosion rate of the MGO/UFP composite coatings (from  $2.93 \times 10^{-5}$  to  $8.59 \times 10^{-3}$  mm/a) was significantly changed in the reduction of  $i_{corr}$  accompanied with more positive  $E_{corr}$  via including MGO suspension.<sup>39</sup> The results were in good agreement with the observed barrier performance of the UFP coating via embedding MGO nanohybrids compared with GO nanosheets. In this work, increasing GO content to 2% had a significant effect on accelerating the corrosion rate of the MGO/UFP composite coatings because of poor film-forming ability, hard dispersion property of GO and weak adhesion to the metallic substrate.<sup>13,15</sup>

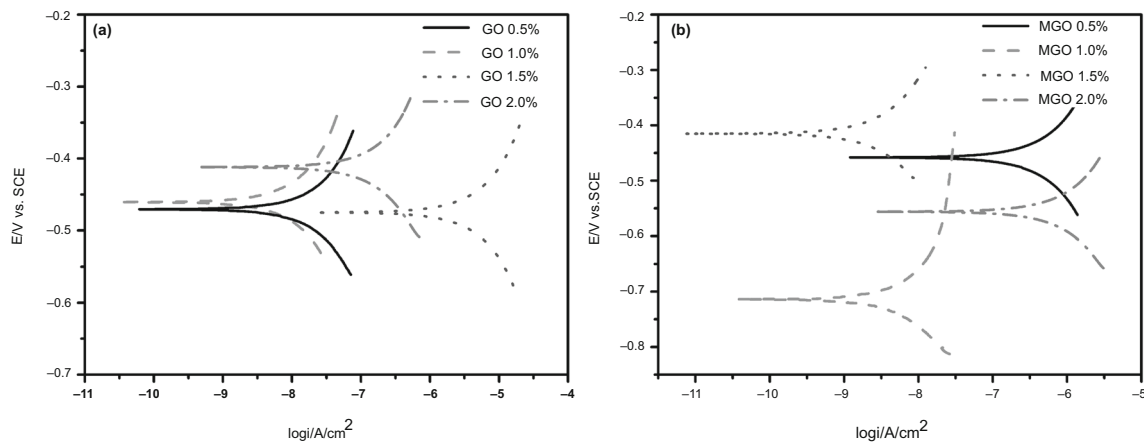


Fig. 7: Potentiodynamic polarization curves for the GO/UFP (a) and MGO/UFP (b) composite coatings containing 0.5, 1.0, 1.5, and 2.0 wt.% GO after immersion in 3.5 wt.% NaCl solution for 14 d

Table 3: Polarization parameters for the GO/UFP and MGO/UFP composite coatings immersed in 3.5 wt.% NaCl solution

Sample	$E_c/mV$	$i_c/A/cm^2$	$R_p/K\Omega/cm^2$	CR/mm/a
GU1	-470.64	$1.88 \times 10^{-8}$	$1.39 \times 10^3$	$2.22 \times 10^{-4}$
GU2	-460.51	$9.64 \times 10^{-9}$	$2.71 \times 10^3$	$1.13 \times 10^{-4}$
GU3	-475.01	$4.16 \times 10^{-6}$	$6.28 \times 10^3$	$4.89 \times 10^{-2}$
GU4	-411.79	$1.51 \times 10^{-7}$	$1.72 \times 10^2$	$1.78 \times 10^{-3}$
MGU1	-458.08	$3.51 \times 10^{-7}$	74.32	$4.13 \times 10^{-3}$
MGU2	-713.90	$5.22 \times 10^{-9}$	$5.00 \times 10^3$	$6.13 \times 10^{-5}$
MGU3	-414.91	$2.49 \times 10^{-9}$	$1.05 \times 10^4$	$2.93 \times 10^{-5}$
MGU4	-556.08	$7.30 \times 10^{-7}$	35.72	$8.59 \times 10^{-3}$

Electrochemical Impedance Analysis

In order to evaluate the effect of GO content and MGO on electrochemical properties and corrosion protection performance of the MGO/UFP composite coatings, there were the Bode and Nyquist plots (Fig. 8) of the GO/UFP and MGO/UFP composite samples with, respectively,  $\log |Z|$  vs.  $\log$  frequency and imaginary impedance vs. real impedance as axes.<sup>13</sup> The GO/UFP and MGO/UFP composite samples were tested after immersion in 3.5 wt% NaCl solution for different times.<sup>30</sup>

In Nyquist plots (Figs. 8a and 8b), the GO/UFP and MGO/UFP composite samples were characterized by a capacitive loop in the high frequency range and an inductive loop in the low frequency range, which is supported by the previously published results.<sup>13,40,41</sup> Signals at the larger radius of the arc are related to the greater anticorrosion resistance and more difficult electrons transfer.<sup>13,30</sup>

In this experiment, it could be observed from the Nyquist plots (Figs. 8a and 8b) that the diameters of the capacitive loops for the GO/UFP composite samples (GO, 1.0 wt%) and the MGO/UFP composite samples (GO, 1.5 wt%) were remarkably larger in

comparison with that of the other three samples with GO in their UFP coatings, which suggested the improvement of the corrosion resistance of the samples with the presence of GO and MPS. As expected, when the doping amount of GO and MGO 1.0 wt.% and 1.5 wt.%, respectively, the impedance reached the maximum at the low frequency of 0.01 Hz ( $|Z|_{0.01}$  Hz) in the EIS bode plots (Fig. 8c and Fig. 8d) and phase diagrams (Fig. 8e and Fig. 8f) for the GO/UFP and MGO/UFP coatings. These results demonstrated that the high anti-corrosive property can be obtained after adding GO of 1.0 wt.% and MGO of 1.5 wt.% in the GO/UFP and MGO/UFP coatings, respectively. Apparently, the results showed that the highest corrosion resistance upon GO addition treatment (Fig. 7) was in good agreement with the previous results of the lowest corrosion current densities ( $i_c$ ) in the GO/UFP and MGO/UFP composite coating with GO (1.0, 1.5 wt%) as addition agent (Fig. 7).

To analyze the EIS data for further understanding the corrosion behavior of the GO/UFP and MGO/UFP composite coatings, the proposed equivalent circuit was the following structures:<sup>42,43</sup> (1) the resistance of the solution ( $R_s$ ); (2) the resistance of the outer layer of the GO/UFP and MGO/UFP composite coatings

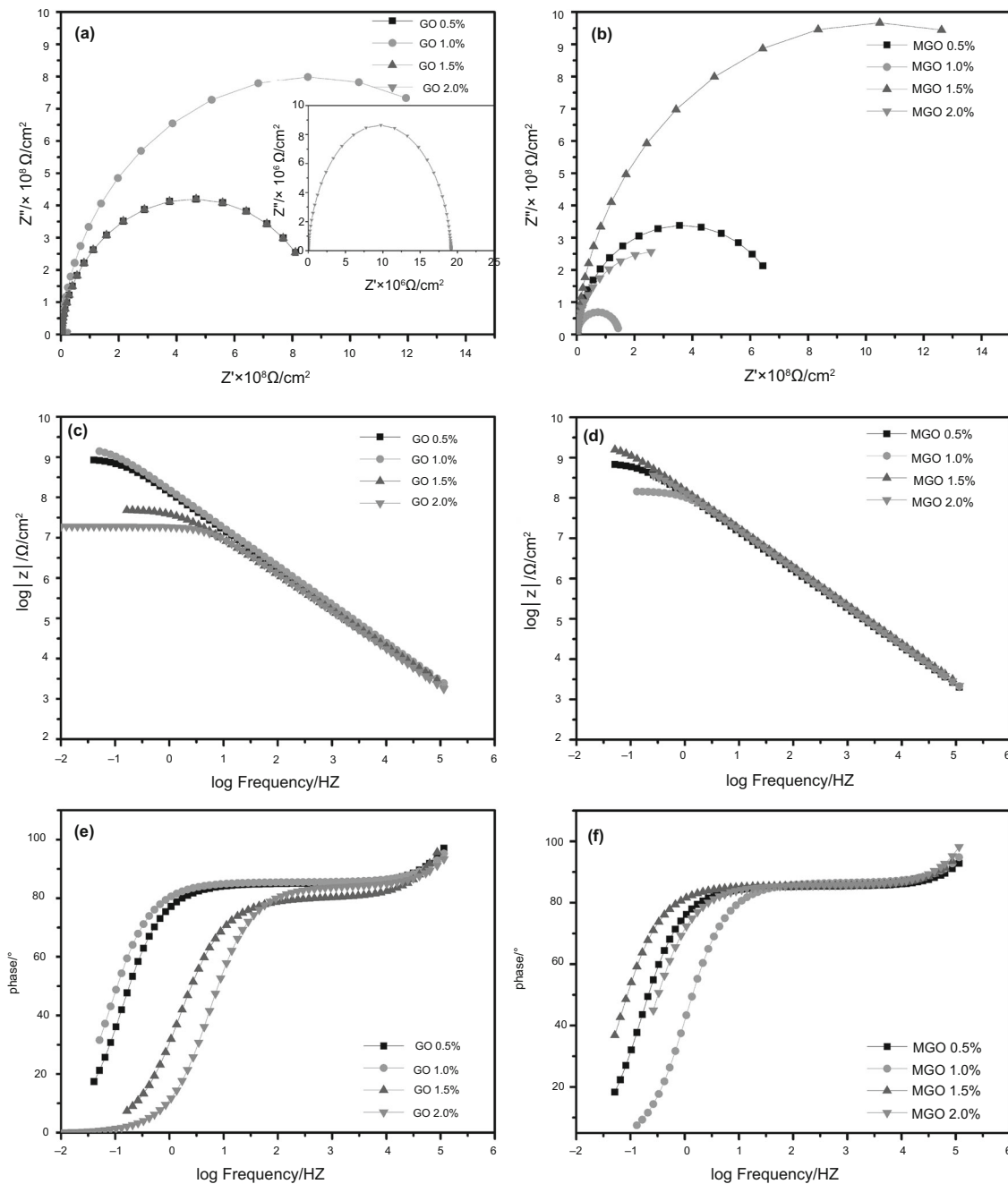


**Fig. 8:** Nyquist plots of the GO/UFP (a) and MGO/UFP (b) composite coating containing different wt.% of GO (0.5, 1.0, 1.5, and 2.0 wt.% GO) after immersion in 3.5 wt.% NaCl solution for 7 days; marker points and solid lines show the experimental and fitted data, respectively. Bode diagrams of the GO/UFP (c) and MGO/UFP (d) composite coating containing different wt.% of GO (0.5, 1.0, 1.5, and 2.0 wt.% GO) after immersion in 3.5 wt.% NaCl solution for 7 days; marker points and solid lines show the experimental and fitted data, respectively. Phase diagrams of the GO/UFP (e) and MGO/UFP (f) composite coating containing different wt.% of GO (0.5, 1.0, 1.5, and 2.0 wt.% GO) after immersion in 3.5 wt.% NaCl solution for 7 days; marker points and solid lines show the experimental and fitted data, respectively

( $R_1$ ); (3) the constant phase elements representing the outer layer ( $CPE_1$ ).

As shown in Table 4, the values of equivalent circuit parameters were derived from the fitting of the EIS data, which demonstrated that the incorporation of

GO into the UFP coating resulted in increasing the  $R_1$ . However, it should be noted that the corrosion resistance of the UFP coatings was mainly determined by the properties of the outer layer ( $R_1$ ). In other words, a higher  $R_1$  value corresponded to higher

corrosion resistance.<sup>44</sup> In this study, it could be observed that both the GU2 and MGU3 coating had higher  $R_1$  than others with GO in their UFP coatings,

**Table 4: The electrochemical parameters extracted from EIS data for the GO/UFP and MGO/UFP composite coatings after immersion in 3.5 wt.% NaCl solution for different times**

Sample	$R_1/K\Omega/cm^2$	CPE <sub>1</sub>	
		$Y_1/\mu\Omega^{-1}m^{-2}S^n$	$n_1$
GU1	9.16E+05	1.29E-03	0.94523
GU2	1.73E+06	1.10E-03	0.94996
GU3	4.98E+04	2.61E-03	0.89071
GU4	1.92E+04	1.87E-03	0.93418
MGU1	7.34E+05	1.36E-03	0.94883
MGU2	1.47E+05	1.09E-03	0.96154
MGU3	2.09E+06	1.12E-03	0.95055
MGU4	5.54E+05	1.21E-03	0.95263

**Table 5: Resistance against chemical medium of the GO/UFP and MGO/UFP composite coatings immersed in 30% H<sub>2</sub>SO<sub>4</sub>, 10% NaOH and 3% NaCl solution at room temperature**

Sample	Chemical medium		
	30% H <sub>2</sub> SO <sub>4</sub>	10% NaOH	3% NaCl
UFP	–	–	–
GU1	+	–	+
GU2	+	–	+
GU3	+	–	+
GU4	+	–	+
MGU1	+	–	+
MGU2	+	–	+
MGU3	+	–	+
MGU4	+	–	+

“+” film without blister, cracking spot, or spoil  
 “–” film with blister, cracking spot, or spoil

which indicated that both the coatings could provide an effective barrier against corrosion ion ingress, particularly the  $R_1$  of the MGO/UFP (GO, 1.5 wt%) composite coating larger than that of the other three samples with GO in their UFP coatings. It indicated that the MGO/UFP composite coating achieved higher corrosion resistance.<sup>45</sup>

In the study, the addition of MGO in the UFP paint liquid by grafting and crosslinking reactions could obtain a high anticorrosive performance MGO/UFP composite coatings, whose main advantages were that the mechanical properties and corrosion resistance for urushiol-formaldehyde were promoted as a novel technique. The results were in good agreement with the observed acid base immersion test. Thus, it is necessary to choose efficient addition agents and apply the novel technology to urushiol coatings with other polymers.

*Anticorrosive performance of the MGO/UFP composite coatings*

In order to characterize the chemical corrosion resistance performance of the MGO/UFP composite coatings, the corrosive experiment in dilute sulfuric acid, sodium hydroxide solution, and sodium chloride solution was carried out. The coated glass plates were immersed in 30% H<sub>2</sub>SO<sub>4</sub>, 10% NaOH, and 3% NaCl solution for 14 days at room temperature, and visual observations were carried out for the loss of light, color, the formation of foam on the coatings surface. The results were recorded to verify the electrochemical impedance spectroscopy (EIS) data (Tables 3 and 4). Compared with UFP surface state, there was no visible superficial phenomenon formed on the MGO/UFP composite films immersed in 30% H<sub>2</sub>SO<sub>4</sub> and 3% NaCl solution, but distinct foam could be observed on the MGO/UFP composite coatings surface immersed in 10% NaOH (Table 5). Therefore, the results indicated that the chemical corrosion resistance of the MGO/UFP composite coatings was enhanced by covering GO as a barrier to the diffusion of acid and saline water.

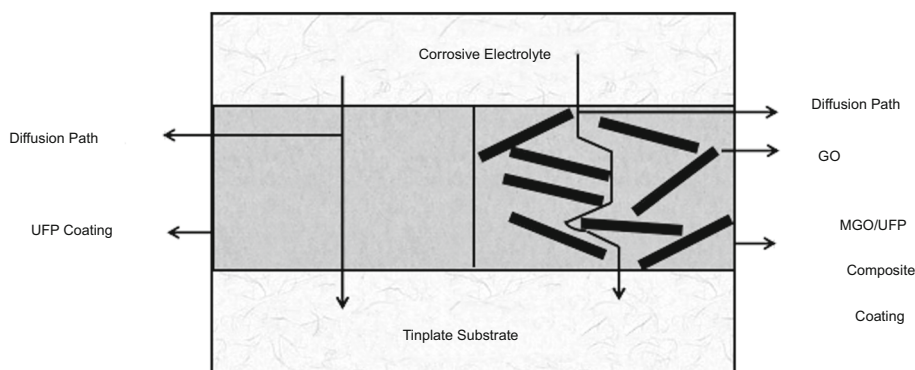


**Fig. 9: Schematic representation of corrosion protection mechanism by the MGO/PUF composite coatings on tinplate substrates**

### Anticorrosion Mechanism

The mechanism of the effect of MGO on the corrosion resistance of UFP between the coating and metallic substrates surface is observed in Fig. 9. There are many reviews in the literature dealing with the basic corrosion protection concepts of water absorption on coating, diffusion of corrosive agents through coating, and reaching corrosive ions at coating/metal interface.<sup>29,46–48</sup>

The electrochemical impedance spectroscopy is applied to find out the protective nature of the composite coating by measuring the resistance ( $R_c$ ) and capacitance ( $C_c$ ) of the composite coating. From the other point of view, the effect of MGO on permeation of corrosive agents through UFP coating is considered. Based on coating capacitance equation (1)<sup>49</sup> and Brasher–Kingsbury's equation (2), it was assumed that the transport of water via polymer coating follows the Fick's law<sup>50,51</sup>:

$$C_c = \varepsilon \varepsilon_0 A / d \quad (1)$$

$$\varphi_w = \frac{\log C_c C_0}{\log \varepsilon_w} \quad (2)$$

In equation (1),  $\varepsilon$  denotes the relative dielectric constant of paint film,  $\varepsilon_0$  the permittivity of the vacuum ( $8.85 \times 10^{-14}$  F/cm),  $A$  the active area, and  $d$  the coating thickness. In equation (2),  $C_c$  is the coating capacitance at immersion time  $t$ ,  $C_0$  is the initial capacitance of dry coating, and  $\varepsilon_w$  is the dielectric constant of water ( $\varepsilon_w \approx 80$ ). Obviously, the volume fraction of water uptake ( $\varphi_w$ ) in organic coatings could be calculated from the capacitance of coatings ( $C_c$ ). It was not difficult to find that the effect of increase in dielectric constant with the permeation of water may increase  $C_c$  value. As a result, variation in capacitance values indicated the water uptake by the polymer film. In the case of MGO/UFP sample, the amount of water uptake increased due to diffusion of corrosive electrolyte through coating. Then, the hydrolysis and condensation reactions of silanols within polymer matrix (UFP) increased the crosslink density of the composite coating which contributed to decreasing of the amount of water uptake with prolonging the immersion time. According to the above-mentioned results, it could be confirmed that MGO acted as barrier and blocked the diffusion path of corrosive agents, leading to corrosion protection.

In the study, it is not difficult to find that the corrosion protection efficiency of the MGO/UFP composite coatings increases remarkably by adding only 1.5 wt% GO and 2.0 wt% MPS. Thus, the result indicated that the MGO/UFP composite coating exhibited the anticorrosive property of metallic substrates via bending the diffusion pathway of penetrant species in the UFP coating matrix and improving the coating adhesion on metallic substrate.<sup>31</sup>

### Conclusion

MGO/UFP composite coatings were successfully prepared through solution blending utilizing a mixture of MGO and UFP. It was found that the chemical grafting of silanes molecules MPS onto the GO surface enhanced the dispersion and compatibility of GO with UFP. The addition of GO in the appropriate amount was implied as an effective method to simultaneously improve the thermal stability, physico-mechanical property. At 1.5 wt% and above, the MGO/UFP composite coating derived from the reaction between MGO and UFP performed as a major anticorrosion coating, which could provide a more effective barrier against corrosive ions ingress. Above 2.0 wt%, increasing GO content had a significant effect on accelerating the corrosion rate, which could inhibit the dispersion of GO and the film-forming ability.

**Acknowledgments** The authors are grateful to the financial support from National Key R&D Program of China (Grant No. 2016YFD0600806) and Excellent Young Teachers Cultivation Program of College of Forestry in Northwest A&F University.

**Open Access** This article is distributed under the terms of the Creative Commons Attribution 4.0 International License (<http://creativecommons.org/licenses/by/4.0/>), which permits unrestricted use, distribution, and reproduction in any medium, provided you give appropriate credit to the original author(s) and the source, provide a link to the Creative Commons license, and indicate if changes were made.

### References

- Lu, R, Ebata, N, Zhang, FL, Miyakoshi, T, "Development of a New Type Lacquer Based on Rhus Vernicifera Sap with Chitosan." *Prog. Org. Coat.*, **77** 439–443 (2014)
- Bai, WB, Lin, JH, "Characterisation of Urushiol Formaldehyde Polymer/Multihydroxyl Polyacrylate /SiO<sub>2</sub> Nanocomposites Prepared by the Sol–Gel Method." *Prog. Org. Coat.*, **71** 43–47 (2011)
- Xu, YL, Tong, ZQ, Xia, JR, Hu, BH, Lin, JH, "Urushiol-Formaldehyde Polymer Microporous Films with Acid–Alkali Resistance Property: Effects of Formation Conditions on Surface Morphologies." *Prog. Org. Coat.*, **72** 586–591 (2011)
- Ma, HX, Xu, ZB, Qiu, JJ, Liu, CM, "Synthesis of Artificial Urushi Via Ring-Opening Reaction of Benzoxazine with Renewable Cardanol." *Polymer*, **132** 41–50 (2017)
- Ping, T, Stevens, B, Devlaming, I, Grunlan, JC, "Polymere-graphene Oxide Quadlayer Thin-Film Assemblies with Improved Gas Barrier." *Langmuir*, **21** 5919–5927 (2015)
- Liu, R, Arabale, G, Kim, J, Sun, K, Lee, Y, "Graphene Oxide Membrane for Liquid Phase Organic Molecular Separation." *Carbon*, **77** 933–938 (2014)
- Hermanova, S, Zarevucka, M, Bousa, D, Pumera, M, Sofer, Z, "Graphene Oxide Immobilized Enzymes Show High Thermal and Solvent Stability." *Nanoscale*, **13** 5852–5858 (2015)

8. Goh, PS, Ismail, AF, “Graphene-Based Nanomaterial: The State-of-the-Art Material for Cutting Edge Desalination Technology.” *Desalination*, **356** 115–128 (2015)
9. Kim, HW, Miura, Y, Macosko, CW, “Graphene/Polyurethane Composites for Improved Gas Barrier and Electrical Conductivity.” *Chem. Mater.*, **22** 3441–3450 (2010)
10. Tang, J, Yao, W, Li, W, Xu, J, Jin, L, Zhang, J, Xu, Z, “Study on a Novel Composite Coating Based on PDMS Doped with Modified Graphene Oxide.” *J. Coat. Technol. Res.*, (2017). <https://doi.org/10.1007/s11998-017-9991-9>
11. Carrasco-Valenzuela, L, Zaragoza-Contreras, EA, Vega-Rios, A, “Synthesis of Graphene Oxide/Poly (3,4-ethylenedioxythiophene) Composites by Fenton’s Reagent.” *Polymer*, **130** 124–134 (2017)
12. He, LH, Zhao, Y, Xing, LY, Liu, PG, Wang, ZY, Zhang, YW, Liu, XF, “Preparation of Phosphonic Acid Functionalized Graphene Oxide-Modified Aluminum Powder with Enhanced Anticorrosive Properties.” *Appl. Surf. Sci.*, **411** 235–239 (2017)
13. Zhu, K, Li, XR, Wang, HH, Li, JY, Fei, GQ, “Electrochemical and Anti-Corrosion Behaviors of Water Dispersible Graphene/Acrylic Modified Alkyd Resin Latex Composites Coated Carbon Steel.” *J. Appl. Polym. Sci.*, **134** 1–12 (2017)
14. Dun, YC, Zuo, Y, “Preparation and Characterization of a GPTMS/Graphene Coating on AA-2024 Alloy.” *Appl. Surf. Sci.*, **416** 492–502 (2017)
15. Shi, JJ, Ma, WS, Lin, XD, “Synthesis and Characterization of Functionalized Graphene with KH-570.” *Chin. J. Inorg. Chem.*, **28** 131–136 (2012)
16. Kumari, S, Panigrahi, A, Singh, SK, Pradhan, SK, “Enhanced Corrosion Resistance and Mechanical Properties of Nanostructured Graphene-Polymer Composite Coating on Copper by Electrophoretic Deposition.” *J. Coat. Technol. Res.*, (2017). <https://doi.org/10.1007/s11998-017-0001-z>
17. Marks, JG, DeMelfi, T, McCarthy, MA, Witte, EJ, Castagnoli, N, Epstein, WL, Aber, RC, “Dermatitis from Cashew Nuts.” *J. Am. Acad. Dermatol.*, **10** 627–631 (1984)
18. Li, F, Liu, Y, Qu, CB, Xiao, HM, Hua, Y, Sui, GX, Fu, SY, “Enhanced Mechanical Properties of Short Carbon Fiber Reinforced Polyethersulfone Composites by Graphene Oxide Coating.” *Polymer*, **59** 155–165 (2015)
19. Zhi, MY, Huang, WX, Shi, QW, Ran, K, “Improving Water Dispersibility of Non-covalent Functionalized Reduced Graphene Oxide with L-tryptophan Via Cleaning Oxidative Debris.” *J. Mater. Sci. Mater. Electron.*, **7** 7361–7368 (2016)
20. Sun, Y, Huang, JH, Fang, KJ, “Application of Waterborne Hyperbranched Polyesteramides Dispersant in Dispersion of Pigment.” *Text. Aux.*, **26** 10–14 (2009)
21. Zhu, M, Lerum, MZ, Chen, W, “How to Prepare Reproducible, Homogeneous, and Hydrolytically Stable Aminosilane-Derived Layers on Silica.” *Langmuir*, **28** 416–423 (2012)
22. Chiong, SJ, Goh, PS, Ismail, AF, “Novel Hydrophobic PVDF/APTES-GO Nanocomposite for Natural Gas Pipelines Coating.” *J. Nat. Gas Sci. Eng.*, **42** 190–202 (2017)
23. Zhang, Y, Zhu, Y, Lin, G, Ruoff, RS, Hu, N, “What Factors Control the Mechanical Properties of Poly (dimethylsiloxane) Reinforced with Nanosheets of 3-aminopropyltriethoxysilane Modified Graphene Oxide?” *Polymer*, **54** 3605–3611 (2013)
24. Xu, YL, Xia, JR, Hu, BH, “Controlled Growth of CdS Nanoparticles in Polyurushiol Matrices.” *Prog. Org. Coat.*, **65** 25–29 (2009)
25. Sato, S, Ido, R, Ose, T, Takahashi, Y, Kanehashi, S, Ishimura, T, Honda, T, Miyakoshi, T, Nagai, K, “Transformation of a Kurome Natural Lacquer Film from Glassy to Rubbery Polymer by the Presence of Moisture.” *Prog. Org. Coat.*, **104** 43–49 (2017)
26. Xu, JZ, Chen, C, Wang, Y, Tang, H, Li, ZM, Hsiao, BS, “Graphene Nanosheets and Shear Flow Induced Crystallization in Isotactic Polypropylene Nanocomposites.” *Macromolecules*, **44** 2808–2818 (2011)
27. Guyard, A, Persello, J, Boisvert, J, Cabaneet, B, “Relationship Between the Polymer/Silica Interaction and Properties of Silica Composite Materials.” *J. Polym. Sci. Part B: Polym. Phys.*, **44** 1134–1146 (2006)
28. Haeri, SZ, Ramezanzadeh, B, Asghari, M, “A Novel Fabrication of a High Performance SiO<sub>2</sub>-Graphene Oxide (GO) Nanohybrids: Characterization of Thermal Properties of Epoxy Nanocomposites Filled with SiO<sub>2</sub>-GO Nanohybrids.” *J. Colloid Interface Sci.*, **493** 111–122 (2017)
29. Zhao, JM, Xie, X, Zhang, C, “Effect of the Graphene Oxide Additive on the Corrosion Resistance of the Plasma Electrolytic Oxidation Coating of the AZ31 Magnesium Alloy.” *Corros. Sci.*, **114** 146–155 (2017)
30. Pourhashem, S, Vaezi, MR, Rashidi, A, “Investigating the Effect of SiO<sub>2</sub>-Graphene Oxide Hybrid as Inorganic Nanofiller on Corrosion Protection Properties of Epoxy Coatings.” *Surf. Coat. Technol.*, **311** 282–294 (2017)
31. Pahnke, J, Ruhe, J, “Attachment of Polymer Films to Aluminium Surfaces by Photochemically Active Monolayers of Phosphonic Acids.” *Macromol. Rapid Commun.*, **25** 1396–1401 (2004)
32. Ramezanzadeh, B, Ahmadi, A, Mahdavian, M, “Enhancement of the Corrosion Protection Performance and Cathodic Delamination Resistance of Epoxy Coating Through Treatment of Steel Substrate by a Novel Nanometric Sol-Gel Based Silane Composite Film Filled with Functionalized Graphene Oxide Nanosheets.” *Corros. Sci.*, **109** 182–205 (2016)
33. Chen, J, Yao, B, Li, C, Shi, G, “An Improved Hummers Method for Eco-Friendly Synthesis of Graphene Oxide.” *Carbon*, **64** 225–229 (2013)
34. Boro, U, Karak, N, “Tannic Acid Based Hyperbranched Epoxy/Reduced Graphene Oxide Nanocomposites as Surface Coating Materials.” *Prog. Org. Coat.*, **104** 180–187 (2017)
35. Maeztu, JD, Rivero, PJ, “Effect of Graphene Oxide and Fluorinated Polymeric Chains Incorporated in a Multilayered Sol-Gel Nanocoating for the Design of Corrosion Resistant and Hydrophobic Surfaces.” *Appl. Surf. Sci.*, **419** 138–149 (2017)
36. Odegarda, GM, Clancy, TC, Gates, TS, “Modeling of the Mechanical Properties of Nanoparticle/Polymer Composites.” *Polymer*, **46** 553–562 (2005)
37. Yousefi, N, Gudarzi, MM, Zheng, Q, Lin, X, Shen, X, “Highly Aligned, Ultralarge-Size Reduced Graphene Oxide/Polyurethane Nanocomposites: Mechanical Properties and Moisture Permeability.” *Compos. Part A*, **49** 42–50 (2013)
38. Haeri, SZ, Asghari, M, Ramezanzadeh, B, “Enhancement of the Mechanical Properties of an Epoxy Composite Through Inclusion of Graphene Oxide Nanosheets Functionalized with Silica Nanoparticles Through One and Two Steps Sol-Gel Routes.” *Prog. Org. Coat.*, **111** 1–12 (2017)
39. Singhababu, YN, Sivakumar, B, Singh, JK, Bapari, H, Pramanick, AK, Sahu, RK, “Efficient Anti-Corrosive Coating of Cold-Rolled Steel in a Seawater Environment Using an Oil-Based Graphene Oxide Ink.” *Nanoscale*, **7** 8035–8047 (2015)
40. Yurekturk, Y, Muhaffel, F, Baydogan, M, “Characterization of Micro Arc Oxidized 6082 Aluminum Alloy in an

- Electrolyte Containing Carbon Nanotubes.” *Surf. Coat. Technol.*, **269** 83–90 (2015)
41. Qi, K, Sun, Y, Duan, H, Guo, X, “A Corrosion-Protective Coating Based on a Solution-Processable Polymer-Grafted Graphene Oxide Nanocomposite.” *Corros. Sci.*, **98** 500–506 (2015)
  42. Vermisoglou, C, Giannakopoulou, T, Romanos, G, “Effect of Hydrothermal Reaction Time and Alkaline Conditions on the Electrochemical Properties of Reduced Graphene Oxide.” *Appl. Surf. Sci.*, **358** 100–109 (2015)
  43. Liang, J, Srinivasan, PB, Blawert, C, Dietzel, W, “Comparison of Electrochemical Corrosion Behaviour of MgO and ZrO<sub>2</sub> Coatings on AM50 Magnesium Alloy Formed by Plasma Electrolytic Oxidation.” *Corros. Sci.*, **51** 2483–2492 (2009)
  44. Ma, H, Li, D, Liu, C, Huang, Z, He, D, Yan, Q, Liu, P, Nash, P, Shen, D, “An Investigation of (NaPO<sub>3</sub>)<sub>6</sub> Effects and Mechanisms During Micro-Arc Oxidation of AZ31 Magnesium Alloy.” *Surf. Coat. Technol.*, **266** 151–159 (2015)
  45. Niu, B, Shi, P, Shanshan, E, Wei, D, Li, Q, Chen, Y, “Preparation and Characterization of HA Sol–Gel Coating on MAO Coated AZ31 Alloy.” *Surf. Coat. Technol.*, **286** 42–48 (2016)
  46. Ji, WG, Hu, JM, Liu, L, Zhang, JQ, Cao, CN, “Improving the Corrosion Performance of Epoxy Coatings by Chemical Modification with Silane Monomers.” *Surf. Coat. Technol.*, **201** 4789–4795 (2007)
  47. Wei, H, Ding, D, Wei, S, Guo, Z, “Anticorrosive Conductive Polyurethane Multiwalled Carbon Nanotube Nanocomposites.” *J. Mater. Chem. A.*, **1** 10805–10813 (2013)
  48. Pourhashem, S, Vaezi, MR, Rashidi, A, Bagherzadeh, MR, “Distinctive Roles of Silane Coupling Agents on the Corrosion Inhibition Performance of Graphene Oxide in Epoxy Coatings.” *Prog. Org. Coat.*, **111** 47–56 (2017)
  49. Sathiyarayanan, S, Azim, SS, Venkatachari, G, “A New Corrosion Protection Coating with Polyaniline–TiO<sub>2</sub> Composite for Steel.” *Electrochim. Acta*, **52** 2068–2074 (2007)
  50. Bellucci, F, Nicodemo, L, “Water Transport in Organic Coatings.” *Corros. Sci.*, **49** 235–247 (1993)
  51. Jiang, MY, Wu, LK, Hu, JM, Zhang, JQ, “Silane-Incorporated Epoxy Coatings on Aluminum Alloy (AA2024). Part 1: Improved Corrosion Performance.” *Corros. Sci.*, **92** 118–126 (2015)